Lawrence Berkeley National Laboratory

Title
Overview of secondary neutron production relevant to shielding in space

Permalink
https://escholarship.org/uc/item/1nh2s8n5

Authors
Heilbronn, L.
Nakamura, T.
Iwata, Y.
et al.

Publication Date
2004-12-03

Overview of secondary neutron production relevant to shielding in space[*]

L. Heilbronn[1], T. Nakamura[2], Y. Iwata[3], T. Kurosawa[4], H. Iwase[5], and L.W. Townsend[6]

(1) MS 74-197, Lawrence Berkeley National Laboratory, Berkeley CA, 94720
Email: LHHeilbronn@LBL.gov
(2) Cyclotron and Radioisotope Center, Tohoku University, Aoba, Aramaki, Aoba-ku, Sendai 980-8578, Japan
(3) Department of Accelerator Physics and Engineering, National Institute of Radiological Sciences, 4-9-1 Anagawa, Inage-ku, Chiba 263-8555, Japan
(4) Quantum Radiation Division, National Metrology Institute of Japan, 1-1-1 Umezono, Tsukuba, Ibaraki 305-8568, Japan
(5) Gesellschaft für Schwerionenforschung, Darmstadt, Germany
(6) Department of Nuclear Engineering, Pasqua Engineering Building, University of Tennessee, Knoxville TN 37996-2300

Abstract

An overview of experimental secondary neutron measurements relevant to space-related activities is presented. Stopping target yields and cross section measurements conducted at particle accelerators using heavy ions with energies >100 MeV per nucleon are discussed.

INTRODUCTION

The risk to crew members' health from exposure to Galactic Cosmic Rays (GCR) and Solar Particle Events (SPE) in deep-space missions can be mitigated in part by the placement of additional shielding materials in critical positions. In general, as shielding thickness increases, the overall dose and dose equivalent decrease. However, as shielding increases, the contribution to the dose and dose equivalent from secondary neutrons also increases. For modest amounts of shielding, such as what is found on the International Space Station (ISS), it has been estimated that approximately 30% of the dose received by astronauts comes from albedo neutrons and secondary neutrons created by interactions in the shielding[1]. In thickly shielded scenarios, such as what may be found in Martian or lunar habitats made of local materials, neutrons may comprise over 50% of the dose equivalent[2,3]. Although protons make up 87% of the baryonic component of the GCR flux (with He ions making up 12% and heavier ions making up 1%), calculations have shown that heavy-ion interactions may produce 1/3 of the total neutron flux[4].

Ultimately, the determination of the most effective shielding scenarios and the biological risk to personnel engaged in long-term missions in space depend on transport models coupled with models that predict the biological endpoints of interest. Given the relatively large uncertainties in predicting secondary neutron flux and the biological consequences of exposure to that flux, it is important for GCR transport models to provide predictions of the neutron flux that are as accurate as possible. Currently, transport models such as HETC, PHITS, and SHIELD-HIT are developing the capability to include heavy-ion interactions, and in some cases are already testing those capabilities with comparisons to the available heavy-ion data. Any experimental data in regards to secondary neutron production from GCR-like heavy-ion interactions will provide critical benchmarks for the development of transport models. This paper highlights the secondary neutron production measurements made at heavy-ion accelerators that are applicable to the field of GCR transport.

SCOPE OF EXPERIMENTS

The GCR flux extends in energy from a few tens of MeV per nucleon up to several TeV per nucleon. The majority of the flux lies between 100 MeV/nucleon and 2 GeV/nucleon, with a broad peak in the flux between 200 and 600 MeV/nucleon, independent of ion species[5]. Ion species range in mass from protons up to iron, with trace amounts of ions heavier than iron. In general, ions with an even atomic number greatly outnumber their odd-atomic-number neighbors. Thus, the beams to be used at accelerator facilities should range from He to Fe, with energies of at least 100 MeV/nucleon. In practice, beams with mass greater than Fe are also useful for studies on the projectile mass dependence on neutron yields in heavy-ion collisions, and are included here.

Because heavy-ion interactions take place in the body as well as structural materials, the range of possible target materials goes from hydrogen up to lead. Targets are not limited to elemental materials; composite targets, such as polyethylene and simulated Martian regolith are also used. Thin targets (thin enough to limit the energy loss in the target to 5% or less) are used for cross-section measurements. Targets used in the thick-

target yield experiments are generally thick enough to stop the beam, although energetic charged light secondaries can escape.

Ideally, the neutron energies measured should extend from thermal energies up to a few GeV. In practice, most accelerator-based neutron detection systems are designed for energies above 1 MeV, and the experiments presented here cover that range of neutron energies. Unlike heavy charged-particle secondaries, neutrons are produced in all space, and as such neutrons should be measured between 0° and 180° in the lab.

THICK-TARGET YIELD EXPERIMENTS

Table I shows the known thick-target (stopping-target) neutron-yield experiments that applicable to GCR transport. The beam ions, energy per nucleon, targets and target thicknesses, and references are shown. With the exception of the measurements by Cecil et al.[6], all of the measurements listed in Table I have been done in the last 10 years.

Table I: Beam ions, energies (MeV/nucleon), targets, target thicknesses (cm), and publication references for neutron thick-target yields from heavy-ion interactions.

Beam ion and energy (MeV/nucleon)	Targets (cm)	Ref.
He (100)	C (5.0), Al (4.0), Cu (1.5), Pb (1.5)	7,8
He (155)	Al (8.26)	13
He (160)	Pb (3.937)	6
He (177.5)	C (14.73), H_2O (22.86), Steel (4.445), Pb (3.937)	6
He (180)	C (16.0), Al (12.0), Cu (4.5), Pb (5.0)	7
C (100)	C (2.0), Al (1.0), Cu (0.5), Pb (0.5)	7
C (155)	Al (8.26)	13
C (180)	C (6.0), Al (4.0), Cu (1.5), Pb (1.5)	7
C (400)	C (20.0), Al (15.0), Cu (5.0), Pb (5.0)	7
Ne (100)	C (1.0), Al (1.0), Cu (0.5), Pb (0.5)	9
Ne (180)	C (4.0), Al (3.0), Cu (1.0), Pb (1.0)	9
Ne (400)	C (11.0), Al (9.0), Cu (3.0), Pb (3.0)	9
Si (800)	C (23.0), Cu (6.5)	10
Ar (400)	C (7.0), Al (5.5), Cu (2.0), Pb (2.0)	10
Fe (400)	C (6.0), Al (4.0), Cu (1.5), Pb (1.5)	10
Nb (272)	Nb (1.0), Al (1.27)	12
Nb (435)	Nb (0.51)	12
Xe (400)	C (3.0), Al (2.0), Cu (1.0), Pb (1.0)	10

Cecil et al. measured neutron yields from 160- and 177.5-MeV/nucleon He stopping in a variety of targets (see Table I). Neutrons were measured between 0° and 150°, with neutron low-energy thresholds at 3 to 10 MeV, depending on the angle measured. Results from this experiment were used to modify HIC (and later HETC) calculations to include He particle interactions. In this set of measurements, it was found that the total

yield of neutrons (above 10 MeV) was roughly independent of target material, at about 0.5 neutrons per incoming He ion.

The measurements of Kurosawa et al.[7-10] provide the most extensive set of thick-target neutron yield data. Beams ions ranged in mass from He to Xe, with energies ranging from 100- to 800-MeV/nucleon. For each beam, targets of C, Al, Cu, and Pb were used. Spectra were measured between 0° and 90°, with neutron low-energy thresholds generally between 3 and 10 MeV, depending on the system and angle measured. Figures 1 and 2 show neutron thick-target spectra at the indicated angles from 400 MeV/nucleon Fe stopping in C, Al, Cu, and Pb targets. In general, the spectra in the forward direction have a broad peak at the high-energy end. The peak energy usually occurs at about 60 to 70% of the beam energy per nucleon. As the target mass becomes lighter and the projectile mass increases, the high-energy peak becomes more prominent. For example, the dependence on target mass can be clearly seen comparing the Fe + C system (Fig. 1, left plot) with the Fe + Pb system (Fig. 2, right plot).
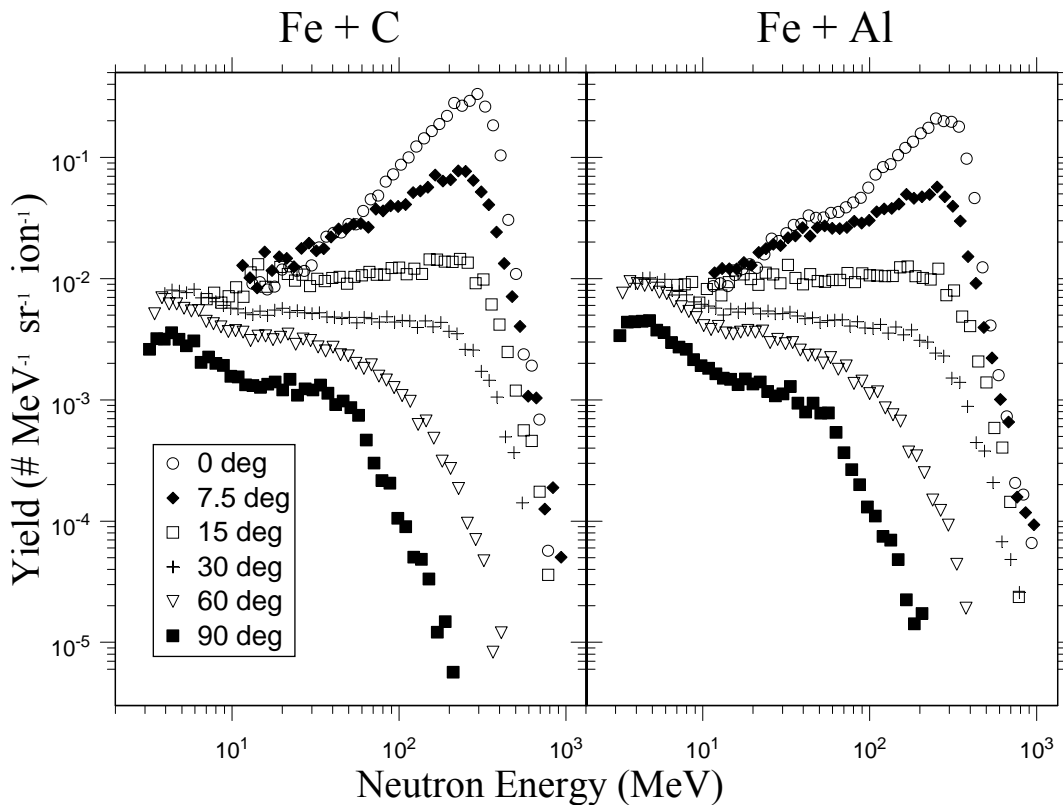

Figure 1: Double differential thick-target yields from 400 MeV/nucleon Fe stopping in a carbon (left plot) and aluminum (right plot).
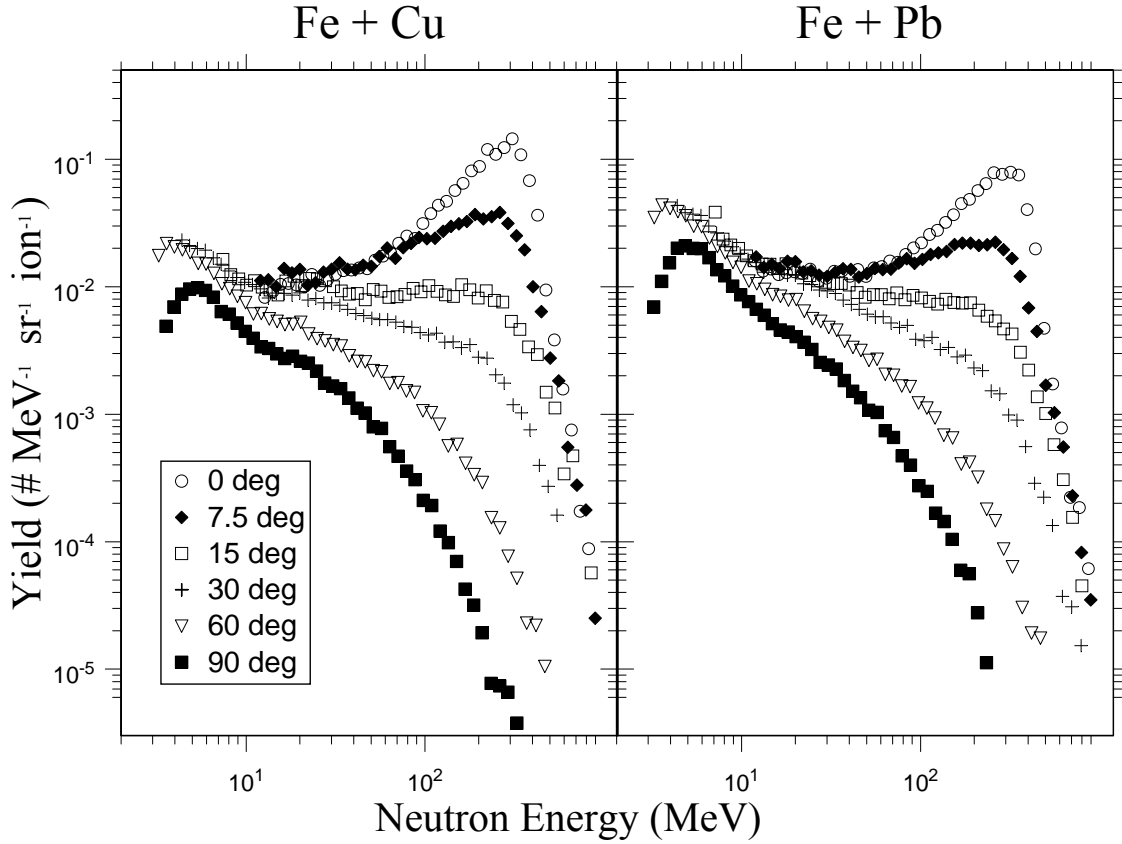
Figure 2: Double differential thick-target yields from 400 MeV/nucleon Fe stopping in a copper (left plot) and lead (right plot).

At energies below 20 MeV, the spectra are dominated by the breakup of the target. Because the target remnant is moving slowly in the lab frame, that source of neutrons is essentially isotropic. As such, target-like neutrons can be seen at all angles. As target mass increases, the relative contribution to the overall spectra from target breakup increases. Again, this feature can be seen by comparing the Fe + C and Fe + Pb spectra at low energies.

HIC calculations[11] of the data (not shown, see Ref. 10) show good agreement for the heavy targets (Cu and Pb), especially at large angles. For the lighter targets, the calculations tend to underestimate the data by as much as a factor of two, especially at the forward angles.

It was found that the Kurosawa results verified the result found by Cecil that the total yield shows very little dependence on target mass. Clearly, there is a dependence on projectile mass, and Kurosawa found that the total yields above 5 MeV integrated between 0° and 90° could be estimated with the following formula:

$$Y = \frac{1.5 \times 10^{-6}}{N_T^{1/3}} E_P^2 \left(A_P^{1/3} + A_T^{1/3} \right)^2 N_P \frac{A_P}{Z_P^2}, \tag{1}$$

where N_T and N_P are the neutron numbers of the target and projectile, A_T and A_P are the mass numbers of the target and projectile, Z_P is the atomic number of the projectile, and E_P is the incident energy per nucleon.

The measurements of Heilbronn et al. show the same general trends seen in the Kurosawa data. The 435- and 272-MeV/nucleon Nb experiments[12] measured neutron yields between 3° and 80°, for neutrons above 20 MeV. The 155 MeV/nucleon He and C experiments[13] measured neutron spectra between 10° and 160° for neutrons above 10 MeV. Heilbronn found that the angular distributions could be fitted with the following equation:

$$Y = a_1 \exp(-a_2\theta) + a_3 \exp(-a_4\theta), \tag{2}$$

where Y is the yield (# per steradian per ion), θ is the angle and a_1, a_2, a_3, and a_4 are fit parameters. The two exponents are thought to represent the contributions to the spectra from the projectile-like source and the decay of the overlap region.

NEUTRON-PRODUCTION CROSS SECTION MEASUREMENTS

Table II shows secondary-neutron production cross-section measurements that are applicable to GCR transport. The beam ions, energy per nucleon, and targets are shown. Where applicable, the references for published data are indicated. All unpublished data has been taken over the last 3 years at HIMAC (Heavy Ion Medical Accelerator in Chiba, Japan).

Table II: Beam ions, energies (MeV/nucleon), targets, and publication references for neutron-production cross-sections from heavy-ion interactions.

Beam ion and energy (MeV/nucleon)	Targets	Ref.
He (135)	C, Al, Cu, Pb	14
He (230)	Al, Cu	
C (135)	C, Al, Cu, Pb	14
C (290)	C, Cu, Pb, marsbar	15
C (400)	Li, C, CH_2, Al, Cu, Pb	15
N (400)	C, Cu	
Ne (135)	C, Al, Cu, Pb	14
Ne (400)	C, Cu, Pb, ISS wall	15
Ne (600)	Li, C, CH_2, Al, Cu, Pb, marsbar	15
Ar (95)	C, Al, Cu, Pb	14
Ar (400)	C, Cu, Pb	15
Ar (560)	C, Cu, Pb, marsbar	15
Fe (500)	Li, CH_2, Al	
Kr (400)	Li, C, CH_2, Al, Cu, Pb	

Xe (400)	C, CH$_2$, Al, Cu, Pb	

   The measurements taken with the 95- and 135-MeV/nucleon beams were performed by Sato et al.[14] at the RIKEN accelerator in Japan. Use of a beam swinger enabled the experimenters to measure cross sections at 0°, as well as 30°, 50°, 80° and 110°. Neutrons were measured for energies above 10 MeV. All other measurements were conducted at HIMAC. Neutron spectra were measured at 5°, 10°, 20°, 30°, 40°, 60°, and 80°. The low-energy neutron-energy thresholds varied between 3 and 10 MeV, depending on the system and angle measured. A subset of that data has been published by Iwata et al.[15] Figure 3 shows spectra measured from 400 MeV/nucleon Ne interacting in an ISS wall segment (the ISS wall is made of 1.89 g/cm^2 of aluminum, 0.218 g/cm^2 of Nomex® honeycomb wall, 0.08 g/cm^2 of Nomex® cloth, 0.06 g/cm^2 Durette® batting, and 0.72 g/cm^2 silicone rubber. The 1.89 g/cm^2 aluminum is a combination of two pieces: an outer "bumper" hull, and an inner pressure wall). The spectra are offset by the indicated factors of 10. The solid histograms show calculations of the data using the PHITS model[16].
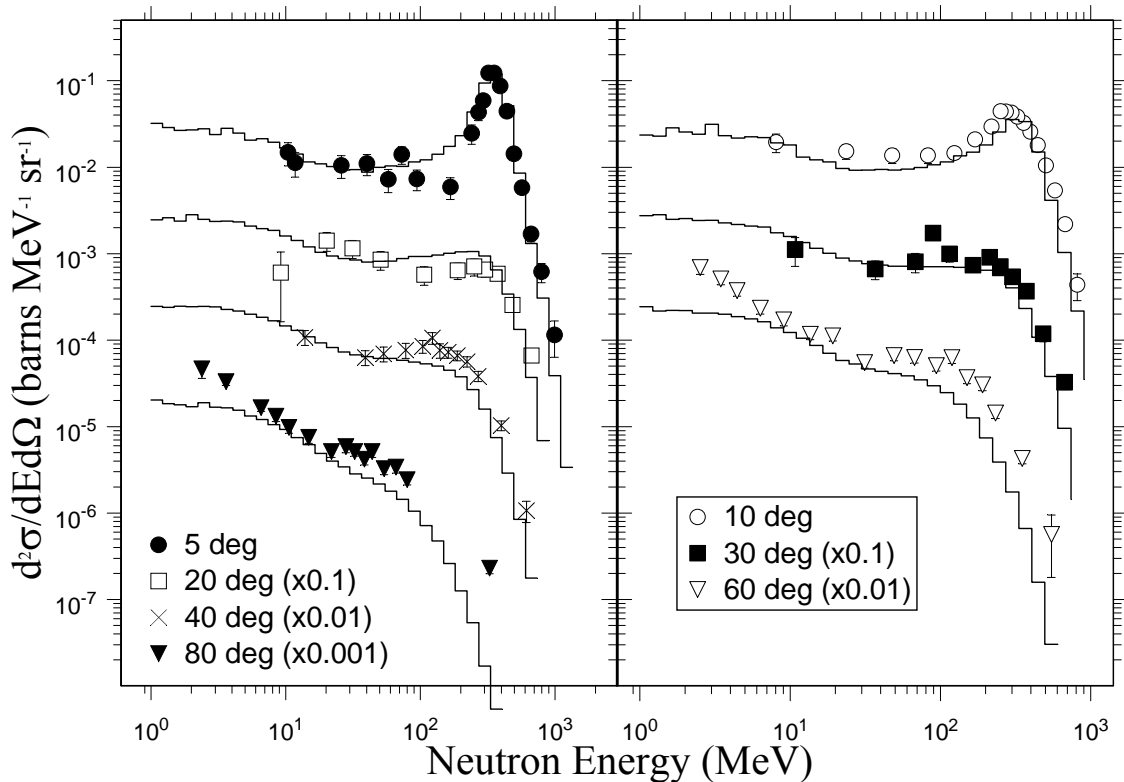

Figure 3. Double-differential neutron spectra from 400 MeV/nucleon Ne + ISS wall, at the indicated laboratory angles. The error bars represent the statistical uncertainty. Results from PHITS calculations are shown with the solid histograms. The spectra and calculations are offset by successive factors of 10, as indicated in the legend.

In general, at forward angles (0° for the RIKEN experiments, 5° for the HIMAC experiments), there is a prominent peak centered near the beam energy per nucleon. As the angle increases, the prominence of the peak decreases to a point at about 20° where the peak is insignificant. The high-energy neutrons in the region of this forward peak come mainly from the breakup of the projectile, along with direct knock-out neutrons from the target. Neutrons are detected at energies 2 to 3 times the beam energy per nucleon, which is a phenomenon attributable to the collective Fermi motion inside the nucleus adding a momentum kick during the collision. At energies below 10 – 20 MeV, the spectra are dominated at all angles by the decay of the target remnant. The exponential behavior of the cross section with energy in this region suggests the target remnant decays by an equilibrium process. At intermediate energies (above 10 to 20 MeV, below the beam energy per nucleon), there is a component that becomes less pronounced as the angle increases. This component is dominated by the pre-equilibrium decay of the overlap region between the projectile and the target.

PHITS model calculations of the data in Fig. 3 show favorable comparisons with the data, especially at forward angles where it is difficult for heavy-ion transport models to fit the data with low-mass targets. There is a general underestimation of the data at backward angles which is also seen with HIC calculations of thick-target data. Figure 4 shows the angular distribution in the 400 MeV/nucleon Ne + ISS wall system. The solid line shows the fit to the data using Eqn. 2 (the dotted and dashed lines show the two components in the fit), and the open symbol shows the PHITS calculation of the angular distribution. The error bars include systematic uncertainties.
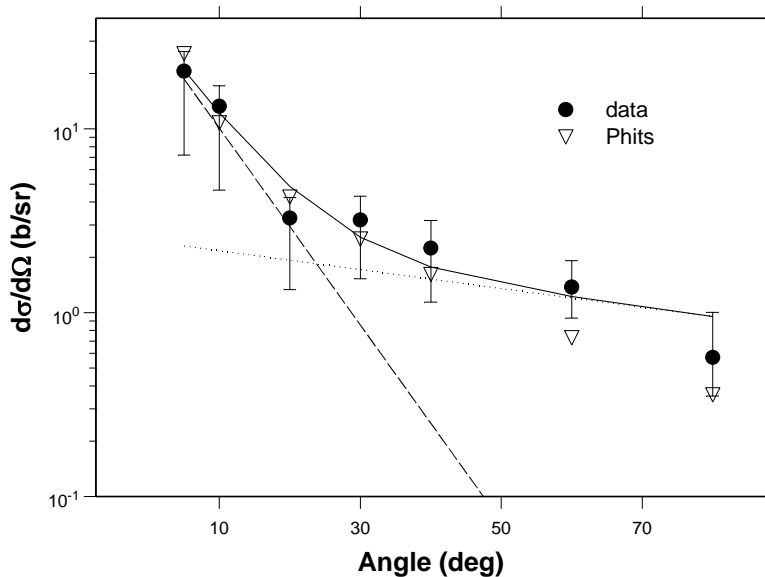

Figure 4. Angular distribution for the 400 MeV/nucleon Ne + ISS wall system. The data is shown with the solid symbols. The error bars include systematical uncertainties. Results from PHITS calculations are shown with the open symbols. The solid, dashed, and dotted lines come from a fit explained in the text.

CONCLUSIONS

Recent measurements performed over the last 10 years have provided developers of GCR transport models with a set of neutron-production cross-section and thick-target yields from heavy-ion interactions. The data span a wide range in beam ion mass, beam energy, and target mass. Comparisons of data with model calculations such as PHITS show, in general, good agreement with the data. However, comparisons of model and thick-target data in systems with low-mass targets are off by as much as a factor of two. Because NASA plans to use shielding materials with light-mass elemental components, this indicates that models will need to improve in those areas.

ACKNOWLEDGEMENTS

References

(1) E.V. Benton and G.D. Badhwar (eds), Prediction and Measurements of Secondary Neutrons in Space, Radiat. Meas. **33** (2001).

(2) L. C. Simonsen et al.; Concepts and strategies for lunar base radiation protection: Prefabricated versus in-situ materials. SAE Technical paper No. 931370, (1992).

(3) L. C. Simonsen, J. E. Nealy, L. W. Townsend and J. W.Wilson, Space Radiation Shielding for a Martian Habitat, SAE Tech. Paper Ser. 911351. (1990).

(4) F.A. Cucinotta, Calculations of Cosmic-Ray Helium Transport in Shielding Materials, *NASA Technical Paper 3354*, (1993).

(5) NCRP (National Council on Radiation Protection and Measurements) Report no. 98, NSRP Publications, 7910 Woodmont Ave., Suite 800, Bethesda, MD 20814 (1989).

(6) R.A. Cecil, B.D. Anderson, A.R. Baldwin, R. Madey, A. Galonsky, P. Miller, L. Young, and F.M. Waterman, Phys. Rev. C **21**, 2471 (1980).

(7) T. Kurosawa, N. Nakao, T. Nakamura, Y. Uwamino, T. Shibata, N. Nakanishi, A. Fukumura, and K. Murakami, Nucl. Sci. Eng **132**, 30 (1999).

(8) T. Kurosawa, T. Nakamura, N. Nakao, T. Shibata, Y. Uwamino, and A. Fukumura, Nucl. Instrum. Meth. **A 430**, 400 (1999).

(9) T. Kurosawa, N. Nakao, T. Nakamura, Y. Uwamino, T. Shibata, A. Fukumura, and K. Murakami, Journ. of Nucl. Sci. Tech. **36**, 41 (1999).

(10) T. Kurosawa, N. Nakao, T. Nakamura, H. Iwase, H. Sato, Y. Uwamino, A. Fukumura, Phys. Rev. C **62**, 044615 (2000).

(11) H. W. Bertini, T. A. Gabriel, R. T. Santoro, O. W. Hermann, N. M. Larson and J. M. Hunt, Oak Ridge National Laboratory Report No. ORNL-TM-4134 (1974).

(12) L. Heilbronn, R. Madey, M. Elaasar, M. Htun, K. Frankel, W.G. Gong, B.D. Anderson, A.R. Baldwin, J. Jiang, D. Keane, M.A. McMahan, W.H. Rathbun, A. Scott, Y. Shao, J.W. Watson, G.D. Westfall, S. Yennello, and W.-M. Zhang, Phys. Rev. C **58**, 3451 (1998).

(13) L. Heilbronn, R.S. Cary, M. Cronqvist, F. Deák, K. Frankel, A. Galonsky, K. Holabird, Á. Horvath, Á. Kiss, J. Kruse, R.M. Ronningen, H. Schelin, Z. Seres, C. E. Stronach, J. Wang, P. Zecher, and C. Zeitlin, Nucl. Sci. Eng. **132**, 1 (1999).

(14) H. Sato, T. Kurosawa, H. Iwase, T. Nakamura, Y. Uwamino, and N. Nakao, Phys. Rev. C **64**, 034607 (2001).

(15) Y. Iwata, T. Murakami, H. Sato, H. Iwase, T. Nakamura, T. Kurosawa, L. Heilbronn, R.M. Ronningen, K. Ieki, Y. Tozawa, and K. Niita, Phys. Rev C **64**, 054609 (2001).

(16) H. Iwase, K. Niita and T. Nakamura, "Development of General-Purpose Particle and Heavy Ion Transport Monte Carlo Code", Journ. Nucl. Sci. Tech., **39**, 1142-1151 (2002).